Nonlocal photopolymerization kinetics including multiple termination mechanisms and dark reactions. Part I. Modeling

Michael R. Gleeson* and John T. Sheridan

UCD School of Electrical, Electronic and Mechanical Engineering, UCD Optoelectronic Research Centre, and The SFI-Strategic Research Cluster in Solar Energy Conversion, College of Engineering, Mathematical and Physical Sciences, University College Dublin, Belfield, Dublin 4, Ireland

**Corresponding author: e-mail: michael.gleeson@ucd.ie*

Received February 5, 2009; revised May 12, 2009; accepted July 14, 2009; posted July 21, 2009 (Doc. ID 107194); published August 19, 2009

The photochemical processes present during free-radical-based holographic grating formation are examined. A kinetic model is presented, which includes, in a more nearly complete and physically realistic way, most of the major photochemical and nonlocal photopolymerization-driven diffusion effects. These effects include: (i) non-steady-state kinetics (ii) spatially and temporally nonlocal polymer chain growth (iii) time varying photon absorption (iv) diffusion controlled viscosity effects (v) multiple termination mechanisms, and (vi) inhibition. The convergence of the predictions of the resulting model is then examined. Comparisons with experimental results are carried out in Part II of this series of papers [J. Opt. Soc. Am. B **26**, 1746 (2009)]. © 2009 Optical Society of America

OCIS codes: 090.7330, 090.2900, 050.1940, 160.5335, 160.5470, 300.1030.

1. INTRODUCTION

The following paper is the first in a series of papers [1] in which we develop and examine a fully comprehensive theoretical representation of the processes that occur during free-radical photopolymerizations. Photopolymer materials [2,3] and the photochemical kinetics associated with them [4] have been studied extensively in the literature of holographic recording. With the growing interest in applications involving photopolymerization mechanisms [5–8], the need for such a theoretical and physically realistic representation is becoming ever more important.

The photochemical processes that are present during photopolymerization are extremely complex [3,4]; however, an understanding of these processes is of utmost importance if a practical model is to be developed. Reviewing the assumptions made in developing the models currently available in the literature [4] leads to the conclusion that the following six physical effects must all be included: (i) non-steady-state kinetics, (ii) spatially and temporally nonlocal polymer chain growth, (iii) time varying photon absorption, (iv) diffusion controlled viscosity effects, (v) multiple termination mechanisms, and (vi) inhibition. Recently, such a model was proposed [9,10]. In this series of papers the model is first developed and then verified experimentally for two significantly different free-radical photopolymer materials [1].

Part I of this series is structured as follows. In Section 2 we briefly review the photochemical processes involved during holographic grating formation and highlight some of the assumptions previously made. In Section 3 the kinetic model, which includes the six effects identified above, is derived. From the resulting set of equations a truncated set of coupled first-order differential equations are then generated. Applying suitable initial conditions, these differential equations are then solved numerically, and simulations of the behavior of the monomer and polymer concentrations are predicted by using typical material parameter values. In Section 4 the calculation of the temporal evolution of the grating refractive index modulation, using the Lorentz–Lorenz relation, is discussed. In Section 5 comparisons of the predictions of the model, calculated with the retention of 4, 8, and 12 concentration harmonics, are made in order to assess the numerical convergence of the model. Finally, in Section 6 we present a brief summary.

In Part II of this series [1], using the model developed here, we examine the photopolymerization effects, both during and post-exposure (dark reactions), in two different photopolymer materials: (i) acrylamide/polyvinyl alcohol (AA/PVA)[3,11] and (ii) an epoxy-resin-based material developed by Trentler *et al.* [12]. The model is used to extract estimates of the physical parameter in both materials.

2. PHOTOCHEMICAL PROCESSES

A. Review of Kinetic Models

Many of the models presented in the literature involve the assumption of a pseudo-steady-state approximation for macroradical concentration [4]. They operate by setting the rate of generation of radicals through photoinitiation, equal to the rate of bimolecular termination. Thus the polymerization rate R_p is given by the expression

$$R_p = k_p M^{\bullet} M = k_p \sqrt{\varphi R_i / k_t} M, \tag{1}$$

where k_p and k_t are the kinetic constants of propagation and termination, respectively, R_i is the rate of decomposi-

tion of the initiator species, φ is the initiator efficiency, and M and $M^\bullet$ are the instantaneous concentrations of monomer and of all macroradicals, respectively. The term *macroradical* refers to all growing polymer chains, i.e., $n>0$ monomer units that have an active tip [13].

When a photopolymer material with a low initiator concentration is exposed to a moderate intensity, the linear dependence among the polymerization rate, the monomer concentration, and the square root dependence on the rate of initiation have been found to agree quite well with experimentally determined rates [3,11]. In this case, the concentration of primary or initiator radicals, $R^\bullet$ (radicals derived directly from photocleavage of the initiator molecule), is very low, and as a result macroradicals, $M_n^\bullet$ [13–16], are much more likely to undergo termination involving another macroradical, i.e., *bimolecular termination* (chain–chain), rather than termination with a primary radical, i.e., *primary termination* (chain–primary radical). Under these conditions, the steady-state assumption is valid, and Eq. (1) describes the polymerization kinetics well.

However, studies have shown [17–19] that at high initiation rates the dependence on initiation drops below that predicted by the square root dependence in Eq. (1). In this case the steady-state assumption is violated, and the deviation from the ideal kinetic behavior described by Eq. (1) becomes pronounced. These effects have been attributed to a phenomenon known as primary radical termination, i.e., *primary termination* [15,17–19]. At these higher initiation rates, there is a significantly larger primary radical concentration, which, as a result, increases the likelihood of primary termination. Furthermore, since the primary radicals can act to limit the buildup of macroradicals, they can effectively reduce the increase in the polymerization rate that is normally seen during the autoacceleration process [19] (see Subsection 2.B).

To proceed, we begin by presenting a consistent set of chemical reaction equations, which allow us to

(i) remove the steady-state approximation for macroradical concentration,
(ii) include spatially and temporally nonlocal polymer chain growth,
(iii) include time varying photon absorption,
(iv) simultaneously include the effects of both primary, i.e., $R^\bullet$–$M^\bullet$, and bimolecular, i.e., $M^\bullet$–$M^\bullet$, termination,
(v) include the changes in the polymerization kinetic constants caused by increased viscosity,
(vi) include polymerization-inhibiting effects.

B. Reaction Mechanisms

The kinetic model presented in this analysis is based on the following four reaction processes [3,11,13,19–21].

Process I. Initiation.

$$I \xrightarrow{h\nu} 2R^\bullet, \tag{2a}$$

$$R^\bullet + M \xrightarrow{ki} M_1^\bullet, \text{chain initiator}. \tag{2b}$$

Process II. Propagation.

$$M_n^\bullet + M \xrightarrow{kp} M_{n+1}^\bullet, \quad \text{growing polymer chain}. \tag{3}$$

Process III. Termination.

$$M_n^\bullet + M_m^\bullet \xrightarrow{ktc} M_{n+m}, \quad \text{dead polymer}, \tag{4a}$$

$$M_n^\bullet + M_m^\bullet \xrightarrow{ktd} M_n + M_m, \quad \text{dead polymer}, \tag{4b}$$

$$M_n^\bullet + R^\bullet \xrightarrow{ktp} M_nR, \quad \text{dead polymer}. \tag{4c}$$

Process IV. Inhibition.

$$R^\bullet + Z \xrightarrow{k_{z,R^\bullet}} (R + Z^\bullet, \text{ and/or } RZ^\bullet), \quad \text{scavenged radical}, \tag{5a}$$

$$M_n^\bullet + Z \xrightarrow{k_{z,M^\bullet}} (M_n + Z^\bullet, \text{ and/or } M_nZ^\bullet), \quad \text{dead polymer}. \tag{5b}$$

In the above set of chemical equations, I is the initiator concentration, $h\nu$ indicates the energy absorbed from a photon, M is the monomer concentration, Z is the inhibitor concentration, and M_n, M_m, M_{n+m}, M_nR, and $M_nZ^\bullet$ represent polymer species with no active propagating tip, i.e., dead polymers. The term *dead polymer* signifies the cessation of the growth of a propagating macroradical of n monomer repeat units [13], while the term *scavenged radical* signifies the removal of a primary radical [10,11,21–23].

Process I. Initiation. The initiation process involves two steps: the first step is the production of free radicals by homolytic dissociation of the initiator to yield a pair of initiator (primary) radicals, $R^\bullet$, i.e., Eq. (2a). If we consider a grating formed by the interference of two plane waves, the spatial distribution of irradiance is cosinusoidal [10,11,15,16,23], and the equation governing Eq. (2a) for the rate of primary radical production is

$$R_i(x,t) = R_i(t)[1 + V\cos(Kx)] = 2\Phi I_a(t)[1 + V\cos(Kx)], \tag{6}$$

where Φ is the number of primary radicals produced per photon absorbed, the inclusion of the factor of 2 follows the convention that indicates that two primary radicals are produced for every photon absorbed [13], V is the fringe visibility, $K=2\pi/\Lambda$ is the grating vector magnitude, and Λ is the grating period. The time varying absorbed intensity, $I_a(t)$ (Einstein/cm^3 s), is given by an adaptation of the Beer–Lambert equation [10,23,24]

$$I_a(t) = \frac{I_0'}{d}\left\{\frac{[\exp(\varepsilon d A_0) - 1]\exp(-\varepsilon\varphi I_0' t)}{1 + [\exp(\varepsilon d A_0) - 1]\exp(-\varepsilon\varphi I_0' t)}\right\}, \tag{7}$$

where d (cm) is the layer thickness, A_0 (mol/cm^3) is the initial photosensitizer/initiator concentration, φ (mol/Einstein) is the quantum yield, ε (cm^2/mol) is the molar absorption coefficient, and I_0' (Einstein/cm^2 s) is the incident intensity [10,23,24].

The second step in the initiation process is chain initiation, Eq. (2b), in which the primary radicals produced as a result of the absorption of photons react with the monomer to produce the chain initiating species $M_1^\bullet$ [3,11,13–16,19,20]. The kinetic rate constant for this step is k_i ($cm^3\ mol^{-1}\ s^{-1}$), i.e., the chain initiation kinetic constant.

Process II. Propagation. The propagation step described in Eq. (3) shows a monomer being added to a growing macroradical chain of n repeat monomeric units, where the propagation rate kinetic constant is denoted k_p ($cm^3\ mol^{-1}\ s^{-1}$).

Process III. Termination. In Eq. (4) three possible termination reactions are presented. Equations (4a) and (4b) represent the bimolecular termination mechanisms, where two growing macroradicals come together and terminate. This method of termination can occur either by combination (k_{tc}), Eq. (4a), or by disproportionation (k_{td}), Eq. (4b). Since the specific mode of termination does not effect the polymerization kinetics, both will be treated in this analysis by use of a single lumped rate constant, $k_t = k_{tc} + k_{td}$ ($cm^3\ mol^{-1}\ s^{-1}$).

Equation (4c) presents the third possible termination mechanism examined, primary radical termination. In this step, a growing macroradical reacts with a primary radical to form an inactive polymer chain or dead polymer. The kinetic rate constant for this step will in general be different from that for the bimolecular termination step for two main reasons:

(i) The reactivity of the primary radical can be very different from that of the chain end radical (radical reactivity can depend on molecular size [13]).

(ii) The primary radicals will be much more mobile, as they are much smaller than the growing macroradicals, and therefore the diffusion controlled effects (caused by viscosity changes due to polymerization) of the two reactions will be quite different.

In the analysis presented here the effects of primary radical recombination will be neglected, as it has been shown that these events are negligible when compared with other polymerization kinetic reactions [17,25].

The kinetic rate constants k_p and k_t in Eqs.(3), (4a), and (4b), are in general dependent on the viscosity of a photopolymer material. As polymerization proceeds, the resulting increase in viscosity of the material (due to densification and cross linking) can cause a significant reduction in the mobility of large molecules, such as the growing macroradical chains. When the diffusional limitations become large enough to restrict the diffusion of these growing macroradical chains, they can no longer diffuse into close enough proximity to react with other macroradicals, and as a result the termination rate, k_t, decreases. This decrease in termination leads to a buildup in macroradical concentration, which subsequently causes a sudden increase in the rate of polymerization, which is known as autoacceleration (gel or Trommsdorff effect) [15,18,19,26]. Once termination drops below a critical level [18,19,26], a different mechanism will become dominant; this mechanism is known as reaction-diffusion.

Reaction-diffusion-controlled termination arises when termination is controlled by the ability of smaller monomer molecules to diffuse to the restricted active macroradical tips. It occurs when the termination of a macroradical is faster and is more likely to take place because of the continued growth of a propagating chain (until it encounters another macroradical for bimolecular termination) than it is likely to diffuse to and thus locate another macroradical chain for termination by bimolecular termination. Since the controlling step in this termination mechanism relies on macroradical chain growth (propagation through available monomer), the termination kinetic constant becomes dependent on the propagation kinetic constant, as indicated in Eq. (8b) below.

As viscosity effects begin to increase further, the mobility of even small molecules, such as the unreacted monomer, becomes limited. Under these conditions, the monomer can no longer easily diffuse to the reactive sites, and as a result the propagation rate k_p, and consequently the rate of polymerization, decreases. This effect is known as *autodeceleration* [13,18,19,26]. Following the analysis of photopolymerization kinetics presented by Goodner *et al.* [18,19], the effects of viscosity changes on the propagation and termination kinetic constants can be expressed as

$$k_p = \frac{k_{p0}}{1 + \exp\left[A_p\left(\frac{1}{f^v} - \frac{1}{f^v_{cp}}\right)\right]}, \tag{8a}$$

$$k_t = \frac{k_{t0}}{1 + \left\{\frac{R_D k_p M}{k_{t0}} + \exp\left[-A_t\left(\frac{1}{f^v} - \frac{1}{f^v_{ct}}\right)\right]\right\}^{-1}}, \tag{8b}$$

where k_{p0} and k_{t0} are the propagation and termination kinetic constants in the absence of diffusional limitations. In these equations, f^v is the fractional free volume of the system [18,19,26–28], and f^v_{cp} and f^v_{ct} are the critical fractional free volumes at which both propagation and termination begin to be diffusionally controlled. A_p and A_t are the parameters that govern the rate at which propagation and termination rates decrease in the diffusion controlled regions. R_D is the reaction-diffusion parameter, which is defined as the termination kinetic constant in the reaction-diffusion region divided by the product of the propagation kinetic constant and the instantaneous unreacted monomer concentration M [18,19,30,31,29].

As the monomer is converted to polymer, the resulting increase in the material viscosity causes a reduction in the free volume of the material, resulting in diffusional effects. This variation in fractional free volume can be described by using the equation

$$f^v = f^v_m \varphi_m + f^v_p (1 - \varphi_m), \tag{9}$$

where $f^v_m = f^v_{Tgm} + \alpha_m (T - T_{gm})$ and $f^v_p = f^v_{Tgp} + \alpha_p (T - T_{gp})$ [18,30–32]. In these equations f^v_m and f^v_p are the fractional free volumes of pure monomer and pure polymer, respectively (where "pure" refers to the values obtained in the absence of any other material components), α_m and α_p are the thermal coefficients of expansion, T_{gm} and T_{gp} are their glass transition temperatures, f_{Tgm} and f_{Tgp} represent their fractional free volumes at the glass transition

temperatures, and T (K) represents the local temperature [18,19,30–32]. φ_m is the volume fraction of monomer, which decreases during polymerization [15,16,33]. Note that the expressions for the diffusion controlled kinetics of both k_i and k_{tp} ($cm^3\ mol^{-1}\ s^{-1}$) will be of the same form as that presented for k_p in Eq. (8a) [18,19,29].

Process IV. Inhibition. The final reaction mechanism, presented in Eq. (5), is inhibition caused by the reaction of the primary radicals and macroradicals with an inhibitor such as dissolved oxygen in the photopolymer material [11,13,16,21–23,34–36]. These radical-consuming reactions tend to

(i) suppress the creation of macroradicals by scavenging primary radicals, Eq. (5a), and/or
(ii) inhibit the macroradicals that are created, Eq. (5b).

This process therefore acts to stop the production of polymer chains and most obviously causes an inhibition or dead-band period at the start of grating growth. This inhibition period will continue until there is a sufficiently low concentration of inhibitor in the material to allow polymerization to occur [11,13,16,21–23]. The kinetics presented in Eq. (5) are simplified by assuming that $Z^\bullet$, $MZ^\bullet$, and $RZ^\bullet$ do not reinitiate polymerization and also that they terminate without regeneration, i.e., they are removed from any possible future reactions.

Previously [10,11,16], it was assumed that the effect of inhibition during exposure was due solely to the initially dissolved oxygen present within the photopolymer layer. However, when the photopolymer is exposed, the initial concentration of dissolved inhibiting oxygen reacts with the radicals produced in the illuminated regions. This nonuniform irradiance causes inhibitor concentration gradients, and hence a diffusion of oxygen from dark regions to bright regions occurs. As the relative size of oxygen molecules are small compared with the surrounding material, it can be assumed that the oxygen is relatively free to diffuse rapidly, resulting in a one-dimensional standard diffusion equation for the concentration of inhibitor,

$$\frac{dZ(x,t)}{dt} = \frac{d}{dx}\left[D_z \frac{dZ(x,t)}{dx}\right] - k_{z,R^\bullet} Z(x,t) R^\bullet(x,t) - k_{z,M^\bullet} Z(x,t) M^\bullet(x,t), \tag{10}$$

where $Z(x,t)$ is the instantaneous inhibiting oxygen concentration and D_z is the diffusion constant of oxygen in the dry material layer, which in this analysis will be assumed to be time and space independent. The inhibition rate constants, $k_{z,R^\bullet}$ and $k_{z,M^\bullet}$, in the reactions presented in Eqs.(5a) and (5b) will in general have different values (of reactivity) due to the differences in their relative molecular sizes [13]; however, in this analysis, for the sake of simplicity they will be treated as being equal, i.e., $k_z = k_{z,R^\bullet} = k_{z,M^\bullet}$. The initial condition for this diffusion equation is $Z(x,0) = Z_0$, for $-\infty < x < \infty$, where Z_0 is the initial concentration of dissolved oxygen that can be measured by using a dissolved oxygen probe [35]. The inhibition rate constant will not have a significant dependence on free volume, as oxygen is a very small molecule and very mobile; therefore the inhibition rate constant can be expressed as

$$k_z = k_{z,0} \exp(-E_z/RT), \tag{11}$$

where in this equation $k_{z,0}$ ($cm^3\ mol^{-1}\ s^{-1}$) is the Arrhenius pre-exponential factor, $E_z = 18.23 \times 10^3$ ($J\ mol^{-1}$) is the activation energy of oxygen, $R = 8.31$ ($J\ K^{-1}\ mol^{-1}$) is the universal gas constant, and T (K) is the local temperature [36].

3. MODEL DEVELOPMENT

In order to combine the kinetic mechanisms presented in Section 2, a new set of governing coupled differential equations are required. The equation governing the concentration of primary radicals is

$$\frac{dR^\bullet(x,t)}{dt} = R_i(x,t) - k_i R^\bullet(x,t) u(x,t) - k_{tp} R^\bullet(x,t) M^\bullet(x,t) - k_z R^\bullet(x,t) Z(x,t), \tag{12}$$

where $u(x,t)$ is the free-monomer concentration (earlier denoted M). This equation states that the rate of change of primary radical concentration is equal to the amount of primary radicals generated by photon absorption minus the amounts removed by (a) the initiation of macroradicals (b) primary termination with growing polymer chains, and (c) inhibition by oxygen.

Including both types of termination mechanism (primary and bimolecular) and the effects of inhibition, the equation governing macroradical concentration is

$$\frac{dM^\bullet(x,t)}{dt} = k_i R^\bullet(x,t) u(x,t) - 2k_t [M^\bullet(x,t)]^2 - k_{tp} R^\bullet(x,t) M^\bullet(x,t) - k_z Z(x,t) M^\bullet(x,t), \tag{13}$$

where the squared term represents the effects of bimolecular termination. The generation term in this equation appears as the removal term due to macroradical initiation in Eq. (12).

When the layer is exposed to the interference fringe pattern, monomer reacts with the primary radicals produced by photon absorption. The nonuniform irradiance creates monomer concentration gradients, and as a result monomer diffuses from the dark regions to the monomer-depleted exposed regions. This enables us to represent the monomer concentration by using the following one-dimensional diffusion equation:

$$\frac{du(x,t)}{dt} = \frac{d}{dx}\left[D_m(x,t) \frac{du(x,t)}{dx}\right] - k_i R^\bullet(x,t) u(x,t) - \int_{-\infty}^{\infty} G(x,x') F(x',t) u(x',t) dx', \tag{14}$$

where $F(x,t)$ is the polymerization rate and $D_m(x,t)$ represents the monomer diffusion constant. $G(x,x')$ is the nonlocal material spatial response function given by

$$G(x,x') = \frac{1}{\sqrt{2\pi\sigma}} \exp\left[\frac{-(x-x')^2}{2\sigma}\right], \tag{15}$$

where σ is the constant nonlocal response parameter normalized with respect to the grating period, Λ [3,9,11,15,16,37]. This nonlocal response function represents the effect of initiation at location x' on the amount of monomer polymerized at location x [3,16,37]. The initial monomer concentration for $-\infty < x < \infty$ is $u(x,0) = U_0$ (mol/cm^3).

Previously, in [15,38–40], a nonlinear relationship was assumed to exist between the polymerization rate, $F(x,t)$ and the recording intensity. This nonlinearity was accounted for using the parameter γ, resulting in the polymerization rate

$$F(x,t) = F_0[1 + V\cos(Kx)]^{\gamma} = \kappa(I_0)^{\gamma}[1 + V\cos(Kx)]^{\gamma}, \tag{16}$$

where κ was assumed to be a material constant. For visibility $V=1$ and nonlinearity parameter $\gamma=\frac{1}{2}$, the polymerization rate was represented by a Fourier series [41].

As this square root dependence of polymerization rate on the rate of initiation, and therefore irradiance, derives from the steady-state approximation for macroradical concentration [see Eq. (1)], it is necessary to suitably adjust the expression for the polymerization rate so that it is expressed as a function of the solution to the non-steady-state equation for monomer radical concentration, Eq. (13). In this case

$$F(x,t) = k_p M^{\bullet}(x,t), \tag{17}$$

where the effective propagation rate, k_p, is dependent on material viscosity effects. The spatial distribution of the polymerization rate is accounted for by the generation or production of primary radicals in the areas exposed to the cosinusoidal irradiance, Eq. (6). As the generation of both the primary radicals and monomer radicals and the removal of monomer and inhibiting oxygen are dependent on the spatial distribution of exposure irradiance, their concentrations will also be periodic even functions of x. Thus the expressions in Eqs.(10) and (12)–(14) can all be written as Fourier series

$$X(x,t) = \sum_{j=0}^{\infty} X_j(t)\cos(jKx), \tag{18}$$

where X represents $R^{\bullet}$, $M^{\bullet}$, u, Z, and D_m. A set of first-order coupled differential equations can then be obtained by gathering the coefficients of the various cosinusoidal spatial contributions and writing the equations in terms of these time varying spatial harmonic amplitudes. Assuming that harmonics of order greater than $j=3$ are negligible, we obtain sets of first-order coupled differential equations, Eqs.(20)–(23), which must be solved with the following initial conditions:

$$Z_0(t=0) = Z_0,$$

$$u_0(t=0) = U_0,$$

and

$$u_{j>0}(t=0) = R^{\bullet}_{j\geq 0}(t=0) = M^{\bullet}_{j\geq 0}(t=0) = 0. \tag{19}$$

Radical Concentration. Substituting Eqs.(6) and (18), into Eq. (12), we gather the coefficients of the various cosinusoidal spatial contributions. Retaining only the first four concentration harmonic amplitudes, the following first-order coupled differential equations governing the primary radical concentration harmonics, $R^{\bullet}_j$, are derived:

$$\begin{aligned}\frac{dR^{\bullet}_0(t)}{dt} = {} & R_i(t) - k_{tp}\left[M^{\bullet}_0(t)R^{\bullet}_0(t) + \frac{1}{2}M^{\bullet}_1(t)R^{\bullet}_1(t) + \frac{1}{2}M^{\bullet}_2(t)R^{\bullet}_2(t) + \frac{1}{2}M^{\bullet}_3(t)R^{\bullet}_3(t)\right] - k_i\left[R^{\bullet}_0(t)u_0(t) + \frac{1}{2}R^{\bullet}_1(t)u_1(t) + \frac{1}{2}R^{\bullet}_2(t)u_2(t) + \frac{1}{2}R^{\bullet}_3(t)u_3(t)\right] \\ & - k_z\left[R^{\bullet}_0(t)Z_0(t) + \frac{1}{2}R^{\bullet}_1(t)Z_1(t)\right],\end{aligned} \tag{20a}$$

$$\begin{aligned}\frac{dR^{\bullet}_1(t)}{dt} = {} & VR_i(t) - k_{tp}\left\{M^{\bullet}_1(t)R^{\bullet}_0(t) + \left[M^{\bullet}_0(t) + \frac{1}{2}M^{\bullet}_2(t)\right]R^{\bullet}_1(t) + \frac{1}{2}[M^{\bullet}_1(t) + M^{\bullet}_3(t)]R^{\bullet}_2(t) + \frac{1}{2}M^{\bullet}_2(t)R^{\bullet}_3(t)\right\} - k_i\left\{R^{\bullet}_1(t)u_0(t) + \left[R^{\bullet}_0(t) + \frac{1}{2}R^{\bullet}_2(t)\right]u_1(t) + \frac{1}{2}[R^{\bullet}_1(t) + R^{\bullet}_3(t)]u_2(t) + R^{\bullet}_2(t)u_3(t)\right\} \\ & - k_z\left[R^{\bullet}_1(t)Z_0(t) + R^{\bullet}_0(t)Z_1(t) + \frac{1}{2}R^{\bullet}_2(t)Z_1(t)\right],\end{aligned} \tag{20b}$$

$$\begin{aligned}\frac{dR^{\bullet}_2(t)}{dt} = {} & -k_{tp}\left\{M^{\bullet}_2(t)R^{\bullet}_0(t) + \frac{1}{2}[M^{\bullet}_1(t) + M^{\bullet}_3(t)]R^{\bullet}_1(t) + M^{\bullet}_0(t)R^{\bullet}_2(t) + \frac{1}{2}M^{\bullet}_1(t)R^{\bullet}_3(t)\right\} - k_i\left\{R^{\bullet}_2(t)u_0(t) - \frac{1}{2}[R^{\bullet}_1(t) + R^{\bullet}_3(t)]u_1(t) + R^{\bullet}_0(t)u_2(t) + \frac{1}{2}R^{\bullet}_1(t)u_3(t)\right\} - k_z\left\{R^{\bullet}_2(t)Z_0(t) + \frac{1}{2}[R^{\bullet}_1(t) + R^{\bullet}_3(t)]Z_1(t)\right\},\end{aligned} \tag{20c}$$

$$\frac{dR_3^{\bullet}(t)}{dt} = -k_{tp}\left[M_3^{\bullet}(t)R_0^{\bullet}(t) + \frac{1}{2}M_2^{\bullet}(t)R_1^{\bullet}(t) + \frac{1}{2}M_1^{\bullet}(t)R_2^{\bullet}(t) + M_0^{\bullet}(t)R_3^{\bullet}(t)\right] - k_i\left[R_3^{\bullet}(t)u_0(t) + \frac{1}{2}R_2^{\bullet}(t)u_1(t) + \frac{1}{2}R_1^{\bullet}(t)u_2(t) + \frac{1}{2}R_0^{\bullet}(t)u_3(t)\right] - k_z\left[R_3^{\bullet}(t)Z_0(t) + \frac{1}{2}R_2^{\bullet}(t)Z_1(t)\right]. \quad (20d)$$

Macroradical Concentration. Substituting Eqs.(18) into Eq. (13) under the same initial conditions gives the following differential equations governing the harmonic amplitudes of the macroradical concentration, $M_j^{\bullet}$:

$$\frac{dM_0^{\bullet}(t)}{dt} = \frac{k_i}{2}[2R_0^{\bullet}(t)u_0(t) + R_1^{\bullet}(t)u_1(t) + R_2^{\bullet}(t)u_2(t) + R_3^{\bullet}(t)u_3(t)] - k_t[2M_0^{\bullet}(t)^2 + M_1^{\bullet}(t)^2 + M_2^{\bullet}(t)^2 + M_3^{\bullet}(t)^2] - \frac{k_{tp}}{2}[2M_0^{\bullet}(t)R_0^{\bullet}(t) + M_1^{\bullet}(t)R_1^{\bullet}(t) + M_2^{\bullet}(t)R_2^{\bullet}(t) + M_3^{\bullet}(t)R_3^{\bullet}(t)] - k_z[2M_0^{\bullet}(t)Z_0(t) + M_1^{\bullet}(t)Z_1(t)], \quad (21a)$$

$$\frac{dM_1^{\bullet}(t)}{dt} = -2k_t[2M_0^{\bullet}(t)M_1^{\bullet}(t) + M_1^{\bullet}(t)M_2^{\bullet}(t) + M_2^{\bullet}(t)M_3^{\bullet}(t)] - k_{tp}\left[M_1^{\bullet}(t)R_0^{\bullet}(t) + \left[M_0^{\bullet}(t) + \frac{1}{2}M_2^{\bullet}(t)\right]R_1^{\bullet}(t) + \frac{1}{2}[M_1^{\bullet}(t) + M_3^{\bullet}(t)]R_2^{\bullet}(t) + \frac{1}{2}M_2^{\bullet}(t)R_3^{\bullet}(t)\right] + k_i\left\{R_1^{\bullet}(t)u_0(t) + \left[R_0^{\bullet}(t) + \frac{1}{2}R_2^{\bullet}(t)\right]u_1(t) + \frac{1}{2}[R_1^{\bullet}(t) + R_3^{\bullet}(t)]u_2(t) + \frac{1}{2}R_2^{\bullet}(t)u_3(t)\right\} - 2k_z\left[M_1^{\bullet}(t)Z_0(t) + M_0^{\bullet}(t)Z_1(t) + \frac{1}{2}M_2^{\bullet}(t)Z_1(t)\right], \quad (21b)$$

$$\frac{dM_2^{\bullet}(t)}{dt} = -k_t[M_1^{\bullet}(t)^2 + 4M_0^{\bullet}(t)M_2^{\bullet}(t) + 2M_1^{\bullet}(t)M_3^{\bullet}(t)] - k_{tp}\left\{M_2^{\bullet}(t)R_0^{\bullet}(t) + \frac{1}{2}[M_1^{\bullet}(t) + M_3^{\bullet}(t)]R_1^{\bullet}(t) + M_0^{\bullet}(t)R_2^{\bullet}(t) + \frac{1}{2}M_1^{\bullet}(t)R_3^{\bullet}(t)\right\} + k_i\left\{R_2^{\bullet}(t)u_0(t) + \frac{1}{2}[R_1^{\bullet}(t) + R_3^{\bullet}(t)]u_1(t) + R_0^{\bullet}(t)u_2(t) + \frac{1}{2}R_1^{\bullet}(t)u_3(t)\right\} - k_z[2M_2^{\bullet}(t)Z_0(t) + M_1^{\bullet}(t)Z_1(t) + M_3^{\bullet}(t)Z_1(t)], \quad (21c)$$

$$\frac{dM_3^{\bullet}(t)}{dt} = -2k_t[M_1^{\bullet}(t)M_2^{\bullet}(t) + 2M_0^{\bullet}(t)M_3^{\bullet}(t)] - k_{tp}\left[M_3^{\bullet}(t)R_0^{\bullet}(t) + \frac{1}{2}M_2^{\bullet}(t)R_1^{\bullet}(t) + \frac{1}{2}M_1^{\bullet}(t)R_2^{\bullet}(t) + \frac{1}{2}M_0^{\bullet}(t)R_3^{\bullet}(t)\right] + k_i\left[R_3^{\bullet}(t)u_0(t) + \frac{1}{2}R_2^{\bullet}(t)u_1(t) + \frac{1}{2}R_1^{\bullet}(t)u_2(t) + R_0^{\bullet}(t)u_3(t)\right] - k_z[2M_3^{\bullet}(t)Z_0(t) + M_2^{\bullet}(t)Z_1(t)]. \quad (21d)$$

Monomer Concentration. Substituting Eqs.(15) and (18) into Eq. (14), we obtain the following coupled equations for the monomer concentration harmonics, u_j:

$$\frac{du_0(t)}{dt} = -\frac{k_p}{2}[2M_0^{\bullet}(t)u_0(t) + M_1^{\bullet}(t)u_1(t) + k_pM_2^{\bullet}(t)u_2(t) + M_3^{\bullet}(t)u_3(t)] - \frac{k_i}{2}[2R_0^{\bullet}(t)u_0(t) + R_1^{\bullet}(t)u_1(t) + k_pR_2^{\bullet}(t)u_2(t) + R_3^{\bullet}(t)u_3(t)], \quad (22a)$$

$$\frac{du_1(t)}{dt} = -S_1k_p\left\{M_1^{\bullet}(t)u_0(t) + \left[M_0^{\bullet}(t) + \frac{1}{2}M_2^{\bullet}(t)\right]u_1(t) + \frac{1}{2}[M_1^{\bullet}(t) + M_3^{\bullet}(t)]u_2(t) + \frac{1}{2}M_2^{\bullet}(t)u_3(t)\right\} - k_i\left\{R_1^{\bullet}(t)u_0(t) + \left[R_0^{\bullet}(t) + \frac{1}{2}R_2^{\bullet}(t)\right]u_1(t) + \frac{1}{2}[R_1^{\bullet}(t) + R_3^{\bullet}(t)]u_2(t) + R_2^{\bullet}(t)u_3(t)\right\} - K^2\left\{\left[D_{m,0}(t) - \frac{1}{2}D_{m,2}(t)\right]u_1(t) + [D_{m,1}(t) - D_{m,3}(t)]u_2(t) - \frac{3}{2}D_{m,2}(t)u_3(t)\right\}, \quad (22b)$$

$$\frac{du_2(t)}{dt} = -S_2k_p\left\{M_2^{\bullet}(t)u_0(t) + \frac{1}{2}[M_1^{\bullet}(t) + M_3^{\bullet}(t)]u_1(t) + M_0^{\bullet}(t)u_2(t) + \frac{1}{2}M_1^{\bullet}(t)u_3(t)\right\} - k_i\left\{R_2^{\bullet}(t)u_0(t) + \frac{1}{2}[R_1^{\bullet}(t) + R_3^{\bullet}(t)]u_1(t) + R_0^{\bullet}(t)u_2(t) + \frac{1}{2}R_1^{\bullet}(t)u_3(t)\right\} - K^2[D_{m,1}(t)u_1(t) - D_{m,3}(t)u_1(t)$$

$$+ 4D_{m,0}(t)u_2(t) + 3D_{m,1}(t)u_3(t)], \tag{22c}$$

$$\frac{du_3(t)}{dt} = -S_3 k_p \left[M_3^{\bullet}(t)u_0(t) + \frac{1}{2}M_2^{\bullet}(t)u_1(t) + \frac{1}{2}M_1^{\bullet}(t)u_2(t) + M_0^{\bullet}(t)u_3(t) \right] - k_i \left[R_3^{\bullet}(t)u_0(t) + \frac{1}{2}R_2^{\bullet}(t)u_1(t) + \frac{1}{2}R_1^{\bullet}(t)u_2(t) + R_0^{\bullet}(t)u_3(t) \right] - 3K^2 \left[3D_{m,0}(t)u_3(t) + D_{m,1}(t)u_2(t) + \frac{1}{2}D_{m,2}(t)u_1(t) \right], \tag{22d}$$

where $S_i = \exp(-i^2K^2\sigma/2)$ [16,39,40].

Inhibitor Concentration: Combination of Eqs. (18) with Eq. (10) yields similar first-order coupled equations for the oxygen harmonics. However, in this case, because of the high mobility of the oxygen molecules, i.e., $D_z \gg D_m$, it is assumed that a time varying diffusion parameter is not necessary and that only two harmonic amplitudes must be retained:

$$\frac{dZ_0(t)}{dt} = -k_z \left\{ [2M_0^{\bullet}(t) + R_0^{\bullet}(t)]Z_0(t) + \left[M_1^{\bullet}(t) + \frac{1}{2}R_1^{\bullet}(t) \right] Z_1(t) \right\}, \tag{23a}$$

$$\frac{dZ_1(t)}{dt} = -k_z \left\{ [2M_1^{\bullet}(t) + R_1^{\bullet}(t)]Z_0(t) + \left[2M_0^{\bullet}(t) + M_2^{\bullet}(t) + R_0^{\bullet}(t) + \frac{1}{2}R_2^{\bullet}(t) \right] Z_1(t) \right\} - K^2 D_z Z_1(t). \tag{23b}$$

These first-order coupled differential equations are then solved numerically with the initial conditions presented in Eq. (19). The concentration of polymerized monomers (repeat monomer units) after an exposure of duration t is given by

$$N(x,t) = \int_0^t \int_{-\infty}^{+\infty} G(x,x')F(x',t')u(x',t')\,dx'\,dt' = \int_0^t \int_{-\infty}^{+\infty} k_p G(x,x') \sum_{l=0}^{\infty} M_l^{\bullet}(t)\cos(lKx') \times \sum_{j=0}^{\infty} u_j(t)\cos(jKx')\,dx'\,dt, \tag{24}$$

which yields the following first two polymer concentration spatial-harmonic components:

$$N_0(t) = \frac{1}{2}\int_0^t k_p[2M_0^{\bullet}(t')u_0(t') + M_1^{\bullet}(t')u_1(t') + M_2^{\bullet}(t')u_2(t') + M_3^{\bullet}(t')u_3(t')]\,dt', \tag{25a}$$

$$N_1(t) = \frac{S_1}{2}\int_0^t k_p\{2M_1^{\bullet}(t')u_0(t') + [2M_0^{\bullet}(t') + M_2^{\bullet}(t')]u_0(t') + [M_1^{\bullet}(t') + M_3^{\bullet}(t')]u_2(t') + M_2^{\bullet}(t')u_3(t')\}dt'. \tag{25b}$$

In numerically calculating the polymer harmonic concentrations, higher-order harmonics of monomer concentrations, i.e., $u_{j>3}$, are assumed to be negligible. Once the monomer harmonics values are known, the polymer harmonic amplitudes can be calculated by substitution into Eq. (25).

4. DIFFRACTION EFFICIENCY AND REFRACTIVE INDEX MODULATION

During the formation of a thick transmission type holographic phase grating the photopolymerization taking place is typically not observed directly. It is the time varying grating diffraction efficiency, $\eta(t)$, that is measured in real time by probing the grating during formation with light of a wavelength that lies outside the range of absorption of the photosensitizer but replays the grating at the Bragg condition, i.e., is on-Bragg. Using first-order electromagnetic coupled wave theory [42], the relationship between the diffraction efficiency, $\eta(t)$, and the first harmonic of the grating refractive index modulation, $n_1(t)$, is given by

$$\eta(t) = \sin^2\left[\frac{\pi d n_1(t)}{\lambda \cos\theta} \right], \tag{26}$$

where d is the thickness of the material layer, λ is the wavelength of the probe–replay laser, and θ is the on-Bragg angle associated with that wavelength. More rigorous models are available that include multiwave components, higher-order ($n_{i>1}$) grating harmonics, [43], and the effects of nonuniform gratings [44].

In order to theoretically predict the temporal evolution of the refractive index modulation, $n_1(t)$, during holographic exposure, it is necessary to know (a) the refractive index of the material layer before exposure, n_{dark}, (b) the refractive index values of the individual components of the material at the probe wavelength, and (c) their time varying concentrations or volume fractions (see Part II [1]).

We begin by examining the average refractive index of the material layer, n, which is dependent on the refractive indices of the individual material components and their volume fractions. Building on work by Kelly *et al.* [45], this relationship can be expressed by using the Lorentz–Lorenz relation [9,15,16,33,45]:

$$\frac{n^2-1}{n^2+2} = \varphi^{(m)}\frac{n_m^2-1}{n_m^2+2} + \varphi^{(p)}\frac{n_p^2-1}{n_p^2+2} + \varphi^{(b)}\frac{n_b^2-1}{n_b^2+2} + \varphi^{(H)}\frac{n_H^2-1}{n_H^2+2}, \tag{27}$$

where n_m, n_p, n_b, and n_H are the refractive indices of monomer, polymer, background material, and holes, re-

spectively, where it is assumed that $n_H=1$ (i.e., *in vacuo*). $\varphi^{(m)}$, $\varphi^{(p)}$, $\varphi^{(b)}$, and $\varphi^{(H)}$ are the respective volume fractions of these components, where the volume fraction is given by $\varphi_i=x_i v_i/\Sigma_i x_i v_i$, where x_i is the mole fraction and v_i is the molar volume of the ith component. The material is therefore modeled as being made up of monomer, polymer (monomer repeat units), holes, and an unchanging background material. In this way, the collapse [45] (or diffusion [33]) of the holes will result in an overall reduction in volume, but the total volume fraction is by definition conserved [9,15,16,33,45,46],

$$\varphi^{(m)}(t)+\varphi^{(p)}(t)+\varphi^{(b)}(t)+\varphi^{(H)}(t)=1. \tag{28}$$

However, in this paper we have neglected all material swelling and shrinkage effects [15,16,33,45], and therefore the concentration of holes is assumed negligible. Thus, the temporal evolution of the index modulation can be written as [15,33]

$$n_1(t)=\frac{(n_{\text{dark}}^2+2)^2}{6n_{\text{dark}}}\left[\varphi_1^{(m)}(t)\left(\frac{n_m^2-1}{n_m^2+2}-\frac{n_b^2-1}{n_b^2+2}\right)+\varphi_1^{(p)}(t)\times\left(\frac{n_p^2-1}{n_p^2+2}-\frac{n_b^2-1}{n_b^2+2}\right)\right], \tag{29}$$

where n_{dark} is the refractive of the material before exposure. $\varphi_1^{(m)}(t)$ and $\varphi_1^{(p)}(t)$ are the time varying first-harmonic volume fraction components of monomer and polymer, respectively, values of which are obtained by solving Eqs.(22)–(25). At grating growth saturation, when there is no monomer left to be polymerized, i.e., $\varphi_1^{(m)}=0$, Eq. (29) reduces to $n_1(t=t_{\text{sat}})\propto\varphi_1^{(p)}(t_{\text{sat}})$.

5. THEORETICAL MODEL PREDICTIONS

The predictions of the model presented in Section 3 are now discussed. Numerical results describing the behavior of the monomer and polymer concentrations are examined, and $n_1(t)$ is then calculated by using Eq. (29). Comparisons of the results of simulations performed retaining 4, 8, and 12 harmonics are made in order to assess the numerical convergence of the method.

Continuous Exposures

In Part II [1], the general photokinetic model is applied to characterize photopolymer material behavior. Before carrying out this procedure we examine the general behavior predicted by our model.

In all the theoretical simulations presented here, it is assumed that the effect of time varying viscosity changes is negligible. As a result the kinetic parameter values chosen for k_p, k_t, k_{tp}, k_z, k_i, and D_m are assumed constant and are given appropriate values or assigned search ranges (in the case of numerical fitting) that are typical for materials similar to AA/PVA photopolymers [13–16,18,19].

All analyses assume layers of thickness $d=100$ μm, exposed with an average incident intensity of $I_i=2$ mW/cm^2. In order to predict the time variation of absorbed intensity during exposure, $I_a(t)$, in Eq. (7), and thus the generation of primary radicals with time, it is necessary to convert the exposure intensity, I_0', into the appropriate units, (Einstein/cm^2 s), by using

$$I_0'=I_i\left(\frac{\lambda}{N_a hc}\right)T_{sf}. \tag{30}$$

In this equation $\lambda=532$ nm is the wavelength of the exposing light, $N_a=6.02\times10^{23}$ mol^{-1} is Avogadro's constant, $c=3\times10^8$ ms^{-1} is the speed of light, $h=6.62\times10^{-34}$ Js is Plank's constant, and T_{sf} is an experimentally estimated loss parameter that takes into account Fresnel and scatter losses [10,16,24].

Since all the simulations presented in this section are generated assuming the same exposure intensity and material thickness, the values used to predict the time variation in absorbed intensity, using Eq. (7), are as follows: $\varepsilon=2\times10^8$ cm^2/mol, $\varphi=0.021$ mol/Einstein, and $T_{\text{sf}}=0.74$. $\Phi=0.2$ is the number of radicals produced per photon absorbed, Eq. (6). These values appear in the literature [10,16] and were estimated from fits to standard AA/PVA experimental data.

The set of four harmonic coupled differential equations presented in Section 3, i.e., Eqs. (20), (21), and (23), combined with Eqs. (25), (26), and (29), are solved for the initial conditions given in Eq. (19), with $U_0=2.83\times10^{-3}$ mol/cm^3 and $Z_0=1\times10^{-7}$ mol/cm^3. The other parameters used are as follows: $k_p=1.6\times10^6$ cm^3 mol^{-1} s^{-1}, $k_t=9\times10^7$ cm^3 mol^{-1} s^{-1}, $k_{\text{tp}}=1\times10^{11}$ cm^3 mol^{-1} s^{-1}, $k_i=5\times10^7$ cm^3 mol^{-1} s^{-1}, $D_m=2\times10^{-11}$cm^2 s^{-1}, $k_{z,0}=5\times10^8$ cm^3 mol^{-1} s^{-1}, and $D_z=5\times10^{-8}$cm^2 s^{-1}. The spatial frequency assumed in these simulations is 1000 lines/mm; the parameter S_1, which represents the effect of nonlocality in the coupled differential equations, was chosen to have a value of $S_1=0.94$. This corresponds to a nonlocal response length of $\sqrt{\sigma'}=54$ nm [3,9,11,15,16,37].

Plots of the amplitudes of the first two harmonics of the monomer and polymer concentrations, as a function of time, are presented in Figs. 1 and 2, respectively. In both plots the solid curve represents the solutions when four harmonics are retained during the numerical solution of the coupled differential equations, i.e., $R_j^{\bullet}$, $M_j^{\bullet}$, and u_j for $0<j<4$. The short-dashed curves represent the solutions generated with retention of 8 harmonics, and the long-dashed lines represent the solutions generated with 12

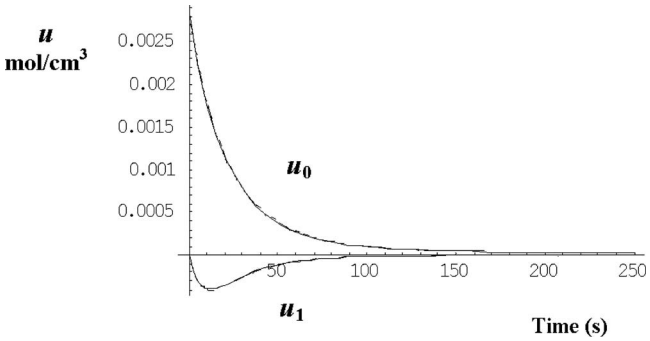

Fig. 1. Predictions of the amplitudes of the first two harmonics of monomer concentration, u_0 and u_1, when 4 (solid curve), 8 (short-dashed curve), and 12 (long-dashed curve), harmonics are retained during the simulations.

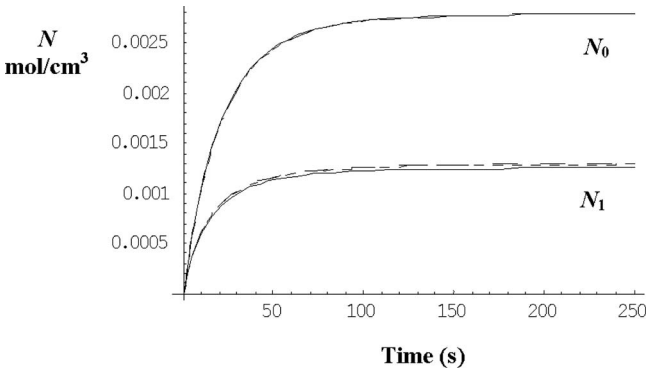

Fig. 2. Amplitudes of polymer concentration, N_0 and N_1, when 4 (solid curve), 8 (short-dashed curve), and 12 (long-dashed curve), harmonics are retained.

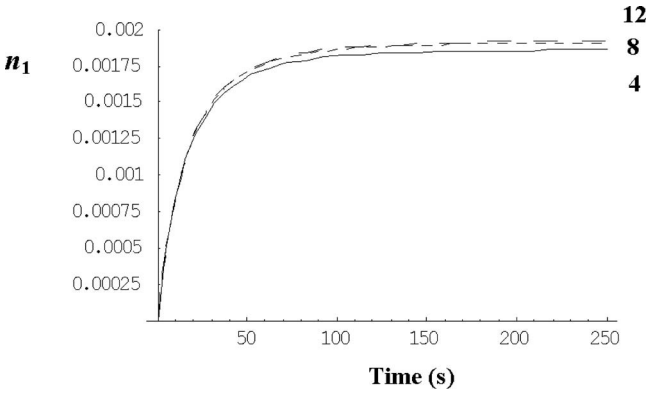

Fig. 3. Comparison of the simulated growth curves for the holographic grating refractive index modulation, for a 2 mW/cm^2 exposure, for 4 (full curve), 8 (short-dashed curve), and 12 (long-dashed curve) harmonics.

harmonics. In all cases two harmonics of the inhibitor concentration are retained, i.e., Z_j for $0<j<1$.

As can be clearly seen in both figures there is a good general agreement between the simulations generated using 4, 8, and 12 harmonics. For both the monomer and the polymer concentration harmonic amplitudes the differences between the 4 and 8 harmonic simulations (2.5% maximum) are greater than those between the 8 and 12 harmonic simulations (1% maximum). This suggests that the system is numerically stable and that the model converges rapidly with the inclusion of higher-order harmonics.

In order to simulate the temporal evolution of grating refractive index modulation for 4, 8, and 12 harmonics, as presented in Fig. 3, we use the refractive indices values $n_m=1.4719$, $n_b=1.4957$, and $n_{\mathrm{dark}}=1.4948$. The refractive index of polymer in AA/PVA was previously estimated to have a value of $n_p=1.52$ [15,16]. The first-harmonic volume fraction components of monomer and polymer $\varphi_1^{(m)}$ and $\varphi_1^{(p)}$ were obtained by using Eq. (27).

6. CONCLUSIONS

Following a detailed discussion of free-radical photopolymerization, a kinetic model, which includes most of the photochemical and mass transport effects that take place during holographic grating formation, has been presented. The model includes the effects of: (i) non-steady-state kinetics, (ii) spatially and temporally nonlocal polymer chain growth, (iii) time varying photon absorption, (iv) diffusion controlled viscosity effects, (v) multiple termination mechanisms, and (vi) inhibition.

The resulting one-dimensional integro-differential nonlocal photopolymerization-driven-diffusion equations are rewritten as a set of coupled first-order differential equations and solved numerically. The model is shown to converge satisfactorily with the retention of a sufficient number of concentration harmonics.

In [4] the development of models in this area is briefly examined, and, as outlined, the model presented here consistently combines several results appearing elsewhere in the literature. However, several completely novel ideas also appear. Two examples of this are (a) the elimination of the steady-state assumption, which makes differentiation between the bimolecular and primary termination mechanisms unnecessary, and (b) the elimination of the separate inclusion of a nonlocal temporal response [15].

Much remains to be done. One possible list of physical processes and effects that are not yet included in this model are given in [4]. However, before further generalization is attempted, it is necessary to compare the predictions of the model to reproducible experimental data for different photopolymer materials. The initial results of such a comparison are presented in Part II of this series of papers [1].

ACKNOWLEDGMENTS

We acknowledge the support of Enterprise Ireland and Science Foundation Ireland through the Research Innovation and Proof of Concept Funds, and the Basic Research and Research Frontiers Programmes. We also thank the Irish Research Council for Science, Engineering and Technology.

REFERENCES

1. M. R. Gleeson, S. Liu, R. R. McLeod, and J. T. Sheridan, "Nonlocal photopolymerization kinetics including multiple termination mechanisms and dark reactions. Part II. Experimental validation," J. Opt. Soc. Am. B **26**, 1746–1754 (2009).
2. G. Manivannan and R. A. Lessard, "Trends in holographic recording materials," Trends Polym. Sci. **2**, 282–290 (1994).
3. J. R. Lawrence, F. T. O'Neill, and J. T. Sheridan, "Photopolymer holographic recording material," Optik **112**, 449–463 (2001).
4. M. R. Gleeson and J. T. Sheridan, "A review of the modelling of free-radical photopolymerisation in the formation of holographic gratings," J. Opt. A **10**, 024008 (2009).
5. S. Harbour, J. V. Kelly, T. Galstian, and J. T. Sheridan, "Optical birefringence and anisotropic scattering in acrylate based holographic polymer dispersed liquid crystals," Opt. Commun. **278**, 28–33 (2007).
6. A. C. Sullivan, M. W. Grabowski, and R. R. McLeod, "Three-dimensional direct-write lithography into photopolymer," Appl. Opt. **46**, 295–301 (2007).
7. J. Zhang, K. Kasala, A. Rewari, and K. Saravanamuttu, "Self-trapping of spatially and temporally incoherent white light in a photochemical medium," J. Am. Chem. Soc. **128**, 406–407 (2006).

8. J. V. Kelly, M. R. Gleeson, C. E. Close, and J. T. Sheridan, "Optimized scheduling for holographic data storage," J. Opt. A **10**, 115203 (2008).
9. M. R. Gleeson, "Analysis of the photochemical kinetics in photopolymers for holographic data storage and hybrid photonic circuits," Ph.D. thesis (University College Dublin, 2008).
10. M. R. Gleeson, S. Liu, S. O'Duill, and J. T. Sheridan, "Examination of the photoinitiation processes in photopolymer materials," J. Appl. Phys. **104**, 064917 (2008).
11. M. R. Gleeson, J. V. Kelly, D. Sabol, C. E. Close, S. Liu, and J. T. Sheridan, "Modelling the photochemical effects present during holographic grating formation in photopolymer materials," J. Appl. Phys. **102**, 023108 (2007).
12. T. Trentler, J. Boyd, and V. Colvin, "Epoxy resin photopolymer composites for volume holography," Chem. Mater. **12**, 1431–1438 (2000).
13. G. Odian, *Principles of Polymerization* (Wiley, 1991).
14. S. Blaya, L. Carretero, R. F. Madrigal, M. Ulibarrena, P. Acebal, and A. Fimia, "Photopolymerization model for holographic gratings formation in photopolymers," Appl. Phys. B **77**, 639–662 (2003).
15. J. V. Kelly, M. R. Gleeson, C. E. Close, F. T. O'Neill, J. T. Sheridan, S. Gallego, and C. Neipp, "Temporal analysis of grating formation in photopolymer using the nonlocal polymerization-driven diffusion model," Opt. Express **13**, 6990–7004 (2005).
16. M. R. Gleeson, D. Sabol, S. Liu, C. E. Close, J. V. Kelly, and J. T. Sheridan, "Improvement of the spatial frequency response of photopolymer materials by modifying polymer chain length," J. Opt. Soc. Am. B **25**, 396–406 (2008).
17. C. H. Bamford, A. D. Jenkins, and R. Johnston, "Termination by primary radicals in vinyl polymerization," Trans. Faraday Soc. **55**, 1451–1460 (1959).
18. M. D. Goodner, H. R. Lee, and C. N. Bowman, "Method for determining the kinetic parameters in diffusion-controlled free-radical homopolymerizations," Ind. Eng. Chem. Res. **36**, 1247–1252 (1997).
19. M. D. Goodner and C. N. Bowman, "Modeling primary radical termination and its effects on autoacceleration in photopolymerization kinetics," Macromolecules **32**, 6552–6559 (1999).
20. H. K. Mahabadi, "Effects of chain-length dependence of termination rate-constant on the kinetics of free-radical polymerization. Part 1. Evaluation of an analytical expression relating the apparent rate-constant of termination to the number-average degree of polymerization," Macromolecules **18**, 1319–1324 (1985).
21. A. Fimia, N. Lopez, F. Mateos, R. Sastre, J. Pineda, and F. Amatguerri, "Elimination of oxygen inhibition in photopolymer system used as holographic recording materials," J. Mod. Opt. **40**, 699–706 (1993).
22. A. K. O'Brien and C. N. Bowman, "Modeling the effect of oxygen on photopolymerization kinetics," Macromol. Theory Simul. **15**(2), 176–182 (2006).
23. M. R. Gleeson, J. V. Kelly, C. E. Close, F. T. O'Neill, and J. T. Sheridan, "Effects of absorption and inhibition during grating formation in photopolymer materials," J. Opt. Soc. Am. B **23**, 2079–2088 (2006).
24. L. Carretero, S. Blaya, R. Mallavia, R. F. Madrigal, A. Belendez, and A. Fimia, "Theoretical and experimental study of the bleaching of a dye in a film-polymerization process," Appl. Opt. **37**, 4496–4499 (1998).
25. T. Manabe, T. Utsumi, and S. Okamura, "Behavior of primary radicals in vinyl polymerization," J. Polym. Sci. **58**(166), 121–146 (1962).
26. C. Decker, B. Elzaouk, and D. Decker, "Kinetic study of ultrafast photopolymerizations reactions," J. Macromol. Sci. Pure Appl. Chem. **A33**(2), 173–190 (1996).
27. A. K. Doolittle, "Studies in Newtonian flow II. The dependence of the viscosity of liquids on free-space," J. Appl. Phys. **22**, 1471–1475 (1951).
28. A. Bondi, "Free volumes and free rotation in simple liquids and liquid saturated hydrocarbons," J. Phys. Chem. **58**, 929–939 (1954).
30. F. L. Marten and A. E. Hamielec, "High-conversion diffusion-controlled polymerization of styrene, Part 1," J. Appl. Polym. Sci. **27**(2), 489–505 (1982).
31. C. N. Bowman and N. A. Peppas, "Coupling of kinetics and volume relaxation during polymerizations of multiacrylates and multimethacrylates," Macromolecules **24**, 1914–1920 (1991).
32. M. L. Williams, R. F. Landel, and J. D. Ferry, "Temperature dependence of relaxation mechanisms in amorphous polymers and other glass-forming liquids," Phys. Rev. **98**, 1549–1549 (1955).
29. K. A. Berchtold, T. M. Lovestead, and C. N. Bowman, "Coupling chain length dependent and reaction diffusion controlled termination in the free radical polymerization of multivinyl (meth)acrylates," Macromolecules **35**, 7968–7975 (2002).
33. I. Aubrecht, M. Miler, and I. Koudela, "Recording of holographic diffraction gratings in photopolymers: Theoretical modelling and real-time monitoring of grating growth," J. Mod. Opt. **45**, 1465–1477 (1998).
34. A. V. Galstyan, R. S. Hakobyan, S. Harbour, and T. Galstian, "Study of the inhibition period prior to the holographic grating formation in liquid crystal photopolymerizable materials," Electronic–Liquid Crystal Communications (2004). Available at http://e_lc.org/Documents/T.V Galstian_2004_05_05_11_13_17.
35. "PreSens GmbH—precision sensing,"http://www.presens.de/html/start.html (retrieved 2007).
36. K. A. Connors, *Chemical Kinetics: The Study of Reaction Rates in Solutions* (Wiley-VCH, 1990).
37. J. T. Sheridan and J. R. Lawrence, "Nonlocal-response diffusion model of holographic recording in photopolymer," J. Opt. Soc. Am. A **17**, 1108–1114 (2000).
38. J. H. Kwon, H. C. Hwang, and K. C. Woo, "Analysis of temporal behavior of beams diffracted by volume gratings formed in photopolymers," J. Opt. Soc. Am. B **16**, 1651–1657 (1999).
39. J. R. Lawrence, F. T. O'Neill, and J. T. Sheridan, "Adjusted intensity nonlocal diffusion model of photopolymer grating formation," J. Opt. Soc. Am. B **19**, 621–629 (2002).
40. J. V. Kelly, F. T. ONeill, J. T. Sheridan, C. Neipp, S. Gallego, and M. Ortuno, "Holographic photopolymer materials: nonlocal polymerization-driven diffusion under nonideal kinetic conditions," J. Opt. Soc. Am. B **22**, 407–416 (2005).
41. J. T. Sheridan, M. R. Gleeson, C. E. Close, and J. V. Kelly, "Optical response of photopolymer materials for holographic data storage applications," J. Nanosci. Nanotechnol. **7**, 232–242 (2007).
42. H. Kogelnik, "Coupled wave theory for thick hologram gratings," Bell Syst. Tech. J. **48**, 2909–2945 (1969).
43. V. L. Colvin, R. G. Larson, A. L. Harris, and M. L. Schilling, "Quantitative model of volume hologram formation in photopolymers," J. Appl. Phys. **81**, 5913–5923 (1997).
44. C. Neipp, A. Belendez, S. Gallego, M. Ortuno, I. Pascual, and J. T. Sheridan, "Angular responses of the first and second diffracted orders in transmission diffraction grating recorded on photopolymer material," Opt. Express **11**, 1835–1843 (2003).
45. J. V. Kelly, M. R. Gleeson, C. E. Close, F. T. O'Neill, J. T. Sheridan, S. Gallego, and C. Neipp, "Temporal response and first order volume changes during grating formation in photopolymers," J. Appl. Phys. **99**, 113105 (2006).
46. R. L. Sutherland, V. P. Tondiglia, L. V. Natarajan, and T. J. Bunning, "Phenomenological model of anisotropic volume hologram formation in liquid-crystal-photopolymer mixtures," J. Appl. Phys. **96**, 951–965 (2004).